Research Article | Vol. 25, No. 26 | 25 Dec 2017 | OPTICS EXPRESS 32767
Optics EXPRESS

Spectral linewidth analysis of semiconductor hybrid lasers with feedback from an external waveguide resonator circuit

YOUWEN FAN,[1,*] ROB E. M. LAMMERINK,[1] JESSE MAK,[1] RUUD M. OLDENBEUVING,[2] PETER J. M. VAN DER SLOT,[1] AND KLAUS-J. BOLLER[1]

[1] *Laser Physics and Nonlinear Optics Group, Faculty of Science and Technology, MESA+ Institute for Nanotechnology, University of Twente, P.O. Box 217, 7500 AE Enschede, The Netherlands*
[2] *LioniX International B.V., P.O. Box 456, 7500 AL Enschede, The Netherlands*
[*] *y.fan@utwente.nl*

Abstract: We present a detailed analysis of a semiconductor hybrid laser exploiting spectral control from an external photonic waveguide circuit that provides frequency-selective feedback. Based on a spatially resolved transmission line model (TLM), we have investigated the output power, emission frequency, and the laser spectral linewidth. We find that, if the feedback becomes weaker, the spectral linewidth is larger than predicted by previous models that are based on a modified mean-field approximation, even if these take a strong spatial variation of the gain into account. The observed excess linewidth is caused by additional index fluctuations that are associated with strong spatial gain variations.

OCIS codes: (130.0130) Integrated optics; (140.5960) Semiconductor lasers; (140.3600) Lasers, tunable; (250.5300) Photonic integrated circuits.

References and links

1. S. Zhang, P. Y. Kam, C. Yu, and J. Chen, "Laser linewidth tolerance of decision-aided maximum likelihood phase estimation in coherent optical M-ary PSK and QAM systems," IEEE Photon. Technol. Lett. **21**(15), 1075–1077 (2009).
2. L. He, Ş. Özdemir, J. Zhu, W. Kim, and L. Yang, "Detecting single viruses and nanoparticles using whispering gallery microlasers," Nat. Nanotech. **6**(7), 428–432 (2011).
3. A. Hemmerich, D. McIntyre, D. Schropp, D. Meschede, and T. Hänsch, "Optically stabilized narrow linewidth semiconductor laser for high resolution spectroscopy," Opt. Commun. **75**(2), 118–122 (1990).
4. Y. Jiang, A. Ludlow, N. Lemke, R. Fox, J. Sherman, L.-S. Ma, and C. Oates, "Making optical atomic clocks more stable with 10^{-16}-level laser stabilization," Nat. Photonics **5**(3), 158–161 (2011).
5. M. Faugeron, M. Tran, O. Parillaud, and M. Chtioui, "High-power tunable dilute mode DFB laser with low RIN and narrow linewidth," IEEE Photon. Technol. Lett. **25**(1), 7–10 (2013).
6. Y. A. Akulova, G. A. Fish, P.-C. Koh, C. L. Schow, P. Kozodoy, A. P. Dahl, S. Nakagawa, M. C. Larson, M. P. Mack, T. A. Strand, C. W. Coldren, E. Hegblom, S. K. Penniman, T. Wipiejewski, and L. A. Coldren, "Widely tunable electroabsorption-modulated sampled-grating DBR laser transmitter," IEEE J. Sel. Topics Quantum Electron. **8**(6), 1349–1357 (2002).
7. C. Henry, "Theory of the linewidth of semiconductor lasers," IEEE J. Quantum Electron. **18**(2), 259–264 (1982).
8. B. Liu, A. Shakouri, and J. E. Bowers, "Passive microring-resonator-coupled lasers," Appl. Phys. Lett. **79**(22), 3561–3563 (2001).
9. T. Kita, K. Nemoto, and H. Yamada, "Silicon photonic wavelength-tunable laser diode with asymmetric Mach-Zehnder interferometer," IEEE J. Sel. Topics Quantum Electron. **20**(4), 344–349 (2014).
10. R. Kazarinov and C. Henry, "The relation of line narrowing and chirp reduction resulting from the coupling of a semiconductor laser to passive resonator," IEEE J. Quantum Electron. **23**(9), 1401–1409 (1987).
11. T. Komljenovic, S. Srinivasan, E. Norberg, M. Davenport, G. Fish, and J. E. Bowers, "Widely tunable narrow-linewidth monolithically integrated external-cavity semiconductor lasers," IEEE J. Sel. Topics Quantum Electron. **21**(6), 214–222 (2015).
12. M. Wu, Y. Lo, and S. Wang, "Linewidth broadening due to longitudinal spatial hole burning in a long distributed feedback laser," Appl. Phys. Lett. **52**(14), 1119–1121 (1988).
13. F. Girardin, G.-H. Duan, and P. Gallion, "Linewidth rebroadening due to nonlinear gain and index induced by carrier heating in strained quantum-well lasers," IEEE Photon. Technol. Lett. **8**(3), 334–336 (1996).

#312314 https://doi.org/10.1364/OE.25.032767
Journal © 2017 Received 31 Oct 2017; revised 27 Nov 2017; accepted 5 Dec 2017; published 15 Dec 2017

Optics EXPRESS

14. S. Srinivasan, M. Davenport, T. Komljenovic, J. Hulme, D. T. Spencer, and J. E. Bowers, "Coupled-ring-resonator-mirror-based heterogeneous III-V silicon tunable laser," IEEE Photon. J. **7**(3), 1–8 (2015).
15. VPIphotonics, "http://www.vpiphotonics.com/Tools/ComponentDesign" .
16. A. Lowery, "New dynamic semiconductor laser model based on the transmission-line modelling method," IEE Proc.-J **134**(5), 281 (1987).
17. W. Hoefer, "The transmission-line matrix method - theory and applications," IEEE Trans. Microw. Theory Techn. **33**(10), 882–893 (1985).
18. Y. Fan, R. M. Oldenbeuving, P. J. M. van der Slot, and K.-J. Boller, "A semiconductor-glass waveguide hybrid laser with ultra-long cavity length," in Proceedings of the 20th Annual Symposium of the IEEE Photonics Society Benelux, (2016), pp. 121–124.
19. T. Chu, N. Fujioka, and M. Ishizaka, "Compact, lower-power-consumption wavelength tunable laser fabricated with silicon photonic wire waveguide micro-ring resonators," Opt. Express **17**(16), 14063–14068 (2009).
20. R. M. Oldenbeuving, E. J. Klein, H. L. Offerhaus, C. J. Lee, H. Song, and K.-J. Boller, "25 kHz narrow spectral bandwidth of a wavelength tunable diode laser with a short waveguide-based external cavity," Laser Phys. Lett. **10**(1), 015804 (2013).
21. J. C. Hulme, J. K. Doylend, and J. E. Bowers, "Widely tunable vernier ring laser on hybrid silicon," Opt. Express **21**(17), 19718–19722 (2013).
22. A. Yariv, "Coupled-mode theory for guided-wave optics," IEEE J. Quant. Electron. **9**(9), 919–933 (1973).
23. T. L. Koch and U. Koren, "Semiconductor lasers for coherent optical fiber communications," J. Lightw. Technol. **8**(3), 274–293 (1990).
24. R. Tang, T. Kita, and H. Yamada, "Narrow-spectral-linewidth silicon photonic wavelength-tunable laser with highly asymmetric Mach-Zehnder interferometer," Opt. Lett. **40**(7), 1504–1507 (2015).
25. C. Henry, "Theory of spontaneous emission noise in open resonators and its application to lasers and optical amplifiers," J. Lightw. Technol. **4**(3), 288–297 (1986).
26. G. Bjork and O. Nilsson, "A tool to calculate the linewidth of complicated semiconductor lasers," IEEE J. Quant. Electron. **23**(8), 1303–1313 (1987).
27. K. Ujihara, "Phase noise in a laser with output coupling," IEEE J. Quant. Electron. **20**(7), 814–818 (1984).
28. S. F. Mingaleev and K. Busch, "Scattering matrix approach to large-scale photonic crystal circuits," Opt. Lett. **28**(8), 619–621 (2003).
29. C. G. H. Roeloffzen, L. Zhuang, C. Taddei, A. Leinse, R. G. Heideman, P. W. L. van Dijk, R. M. Oldenbeuving, D. A. I. Marpaung, M. Burla, and K.-J. Boller, "Silicon nitride microwave photonic circuits," Opt. Express **21**(19), 22937–22961 (2013).
30. L. Zhuang, C. G. H. Roeloffzen, M. Hoekman, K.-J. Boller, and A. J. Lowery, "Programmable photonic signal processor chip for radiofrequency applications," Optica **2**(10), 854–859 (2015).
31. C. K. Madsen and J. H. Zhao, *Optical Filter Design and Analysis: A Signal Processing Approach* (John Wiley & Sons, 1999).
32. Y. Fan, R. M. Oldenbeuving, E. J. Klein, C. J. Lee, H. Song, M. R. H. Khan, H. L. Offerhaus, P. J. M. van der Slot, and K.-J. Boller, "A hybrid semiconductor-glass waveguide laser," Proc. SPIE, vol. 9135, 91351B (2014).
33. B. Bennett, R. A. Soref, and J. del Alamo, "Carrier-induced change in refractive index of InP, GaAs and InGaAsP," IEEE J. Quant. Electron. **26**(1), 113–122 (1990).
34. G. D. Domenico, S. Schilt, and P. Thomann, "Simple approach to the relation between laser frequency noise and laser line shape," Appl. Opt. **49**(25), 4801–4807 (2010).
35. C. T. Santis, S. T. Steger, Y. Vilenchik, A. Vasilyev, and A. Yariv, "High-coherence semiconductor lasers based on integral high-Q resonators in hybrid Si/III-V platforms," Proc. Natl. Acad. Sci. U.S.A. **111**(8), 2879–2884 (2014).
36. L. M. Zhang and J. E. Carroll, "Large-signal dynamic model of the DFB laser," IEEE J. Quantum Electron. **28**(3), 604–611 (1992).
37. K. A. Williams, M. G. Thompson, and I. H. White, "Long-wavelength monolithic mode-locked diode lasers," New J. Phys. **6**(1), 179 (2004).
38. L. A. Coldren, S. W. Corzine, and M. L. Mashanovitch, *Diode Lasers and Photonic Integrated Circuits, 2nd edition* (John Wiley & Sons, 2012).
39. R. Nagarajan, M. Ishikawa, T. Fukushima, R. S. Geels, and J. E. Bowers, "High speed quantum-well lasers and carrier transport effects," IEEE J. Quantum Electron. **28**(10), 1990–2008 (1992).
40. K. A. Williams, P. S. Griffin, I. H. White, B. Garrett, J. E. A. Whiteaway, and G. H. B. Thompson, "Carrier transport effects in long-wavelength multiquantum-well lasers under large-signal modulation," IEEE J. Quantum Electron. **30**(6), 1355–1357 (1994).

1. Introduction

Widely tunable, narrow linewidth diode lasers are of significant relevance, ranging from terrestrial applications such as fiber-optic communications [1] or optical sensing [2], to space-based applications such as laser cooling [3] and atomic clocks [4] in global positioning systems (GPS). In the evolution of such applications, monolithic single-frequency diode laser sources, specifically

Optics EXPRESS

distributed feedback (DFB) lasers and distributed Bragg reflector (DBR) lasers, approach their limits due to a relatively small tuning range [5] and large linewidths at the MHz level [6], the latter caused by the short cavity photon lifetime in these lasers. In comparison, so-called hybrid diode waveguide lasers, which have been subject of recent, extensive research, can offer much longer photon lifetimes, and therefore narrower linewidths, in addition to wider tunability. The concept of such hybrid lasers is based on optically coupling a semiconductor gain medium to a low-loss passive waveguide circuit that provides a significantly extended resonator length and a highly frequency selective feedback. The benefits to be gained with low-loss waveguide feedback circuits are that: a) flexible filtering schemes can be applied which allow for wide wavelength tunability, b) narrow linewidths can be achieved due to increased photon lifetime that is associated with an extended cavity length [7], and that c) such lasers are ideal for integrating into subsequent waveguide circuitry fabricated on the same waveguide chip.

Making use of high-quality intra-cavity microring resonators (MRRs) in the feedback circuit has introduced a new paradigm on how to pursue chip-based narrow linewidth semiconductor laser sources. As opposed to Bragg gratings, the fabrication of MRRs does not demand complicated lithography processes and can provide lower losses. A related important merit of using low-loss MRRs is that they effectively extend the optical length of the laser resonator by an appreciable factor, due to the multiple roundtrips in the MRR [8]. This length extension contributes again to a narrowing of the laser linewidth.

The tuning properties of such hybrid lasers are generally well-understood. However, the laser linewidth remains challenging to predict due to the increased complexity of the cavity design which is ruled by a larger set of experimental parameters. So far, for a coarse estimation of the linewidths of such lasers [9], it is common to employ Henry's theory which is using the mean-field approximation (MFA) corrected with the so-called linewidth enhancement factor, α [7]. However, this approach is rather incomplete since the effect of linewidth narrowing or broadening induced by the spectral selectivity and dispersion of the external feedback [10] is not taken into account.

To overcome these shortcomings, refined models were developed [10] and used for comparison with experimental linewidth data, and qualitative agreement was found [11]. However, still these theories are based upon the mean-field approximation (MFA) in the gain section. Specifically for hybrid lasers this approximation is questionable and can be insufficiently accurate. The reason is that hybrid lasers, depending on the strength of the feedback, may show strong spatial variations of the intensity in the semiconductor gain element which introduces strong variations of the carrier density as well. We note that in monolithic diode lasers with a single cavity of short length such spatial effects [12] and nonlinear gain effects [13] cause an increase of the laser linewidths as compared to mean-field models.

In this work, we present the first modeling of external cavity diode lasers (ECDLs), also called extended cavity diode lasers, that takes into account the complex feedback obtained with waveguide resonator circuits such as in [11] and [14] and that simultaneously takes into account the detailed spatial variation of the diode-internal intensity and carrier density, such as in [12] and [13]. The goal of our detailed modeling is to enable a comparison with the existing simplified theories and, thereby, check their validity under different conditions. To this end, we make use of a commercially available, advanced transmission line model (TLM) [15] which involves spatially resolved rate equations for the complex-valued electric field and spatially resolved rate equations for the carrier density [16, 17] in the active section of the laser cavity that contains the semiconductor optical amplifier. The remaining, external part of the cavity that comprises the linear optical waveguide feedback and spectral filtering circuit is modeled as a complex-valued frequency dependent scattering matrix. A first test of this model has been described in our previous conference publication [18], showing satisfying agreement in terms of linewidth within a factor of about 1.5 in the 20-50 kHz range, with experimental data obtained with a relatively

Optics EXPRESS

short InP-Si_3N_4 waveguide hybrid laser with feedback from two MRRs, and with a fixed optical coupling strength between the InP gain section and the Si_3N_4 waveguide chip. In order to cover different regimes of interest, here we systematically vary this power coupling strength, β, between the InP gain section and the Si_3N_4 waveguide chip. This variation brings the diode internal field and carrier distribution from spatially high uniformity ($\beta \approx 1$ and strong feedback from the waveguide resonators, where the MFA remains justified) towards a strong spatial variation ($\beta \approx 0$ or weak resonator feedback) where a detailed modeling has not been performed so far. The drive current of the diode amplifier is used as an adjustable input parameter because also in a typical experimental investigation the electric drive current can be varied most easily. For each setting of the chip-to-chip coupling efficiency we calculate the power spectral density of the frequency noise from which we derive a value for the laser linewidth, to compare with values obtained with a modified MF theory.

2. Operation principle

The hybrid laser that we model comprises a semiconductor active gain section coupled to a passive external cavity as shown in Fig. 1. For definiteness, as required in a numerical model, and to guide our experimental efforts, we chose a typical InP diode as amplifier while the feedback is provided via a Si_3N_4 waveguide chip.

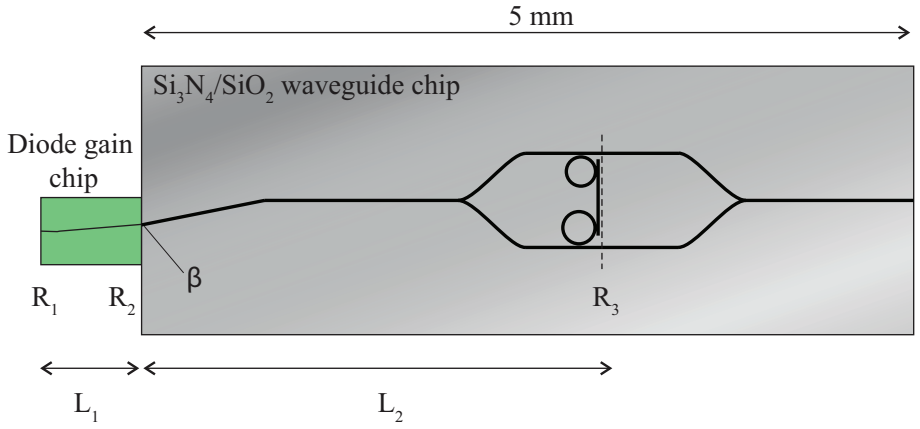

Fig. 1. Schematic representation of the hybrid laser with an active gain section with length L_1 coupled, with power coupling coefficient β, to a passive waveguide section with physical length L_2 (excluding the MRRs). The left facet of the laser diode is highly reflective, R_1, and the right facet is anti-reflection coated combined with a tilt angle of 5°, resulting in an extremely low facet reflectivity ($R_2 \approx 0$). The two MRRs provide an effective power reflectivity R_3 which is frequency dependent.

The laser diode gain section has one high-reflectivity facet with power-reflectivity R_1 and one facet with low power-reflectivity R_2. The overall feedback provided by the Si_3N_4 waveguide chip circuitry is lumped into a frequency dependent power reflectivity, $R_{eff}(\omega)$, which comprises both propagation through the passive straight waveguides and reflection from two microring resonators (MRRs) of slightly different free spectral range (FSR). The two MRRs provide a so-called Vernier mirror, and act as wavelength-selective reflective filters. Wavelength tuning can be achieved via the thermo-optic effect, i.e., by heating of the MRRs, which increases the effective waveguide index and thereby the optical length of the MRRs. Further details about MRR Vernier filters can be found in [19–21].

Radiation generated by spontaneous and stimulated emission in the amplifier chip enters

Optics EXPRESS

the Si_3N_4 waveguide chip with a power coupling coefficient, β, that depends on the overlap (matching) of the mode profiles in the gain waveguide and Si_3N_4 waveguide [22].

In the Si_3N_4 chip, light is first divided by a symmetric 50/50 splitter (Y-junction), and then guided sequentially through the two cascaded MRRs before being combined and fed back to the gain section. For the hybrid laser to oscillate at the frequency of a specific longitudinal mode of the entire cavity, that frequency must also be supported by the gain spectrum of the specific semiconductor material used, and coincide with the transmission spectra of both MRRs. A second symmetric 50/50 splitter (Y-junction) combines the light that passes by the throughputs of the MRRs, which can be used as laser output.

3. Revisiting laser linewidth theories

The currently most complete analytical theory [10, 23] for external cavity diode lasers with spectrally filtered feedback suggests that the linewidth of the hybrid laser, $\Delta\nu$, can be calculated along the following lines: first, the hybrid laser is modeled in the same manner as a solitary Fabry-Perot laser with a back facet field amplitude reflectivity of $r_1 = \sqrt{R_1}$, which is frequency-independent and real-valued. The front facet is given a complex-valued amplitude reflectivity, $r_{eff}(\omega) = r(\omega)exp(-j * \varphi_{eff}(\omega))$. The real-valued amplitude factor in this expression, $r(\omega)$, represents the overall field feedback from the external passive circuit, and is given by

$$r(\omega) = \beta \cdot exp(-\alpha_2 L_2) \cdot r_3(\omega). \tag{1}$$

This expression lumps together various effects, namely the field reflectivity of the pair of ring resonators, $r_3(\omega) = \sqrt{R_3(\omega)}$, the power coupling efficiency, β, and any additional loss that occurs in the external feedback path. The frequency dependent phase, $\varphi_{eff}(\omega)$, takes into account the optical delay that the feedback circuit provides. Specifically, this phase varies with the light frequency because it depends on the detuning from the resonance frequency of the Vernier filter and on other optical parameters of the external feedback path, such as the length of the waveguide to and from the MRRs. After lumping the external feedback into $r_{eff}(\omega)$ for the front facet, $\Delta\nu$ is given by:

$$\Delta\nu = \frac{\Delta\nu_{ST}}{F^2}. \tag{2}$$

In this equation, $\Delta\nu_{ST}$ is the Schawlow-Townes linewidth of the equivalent solitary Fabry-Perot diode laser [23]:

$$\Delta\nu_{ST} = \frac{1}{4\pi} \frac{{v_g}^2 h\nu n_{sp}\gamma_{tot}\gamma_m \left(1+\alpha^2\right)}{P_0\left(1+\frac{r_1}{r(\omega)}\frac{1-r(\omega)^2}{1-R_1}\right)}, \tag{3}$$

i.e., of a diode laser having an amplifier section of length L_1 and having real-valued field reflectivities r_1 and $r(\omega)$.

In Eq. (3), $v_g = c/n_{g1}$ is the group velocity in the diode, h is the Planck constant, ν is the laser emission frequency, n_{sp} is the spontaneous emission factor, γ_{tot} is the total loss (mirror loss plus diode internal loss), $\gamma_m = 1/(2L_1)\ln(1/(R_1 r^2(\omega)))$ is the distributed mirror loss, α is Henry's linewidth enhancement factor, and P_0 is the output power from the back diode facet. This facet was chosen due to its frequency independent transmission such that the output is simply proportional to the laser internal power.

The denominator in Eq. (2) is the so-called linewidth reduction factor which describes laser line narrowing due to the frequency dependency of the external feedback,

$$F = 1 + A + B, \tag{4}$$

Optics EXPRESS

where

$$A = \frac{1}{\tau_{LD}} \left(\frac{d}{d\omega} \varphi_{eff}(\omega) \right), \tag{5}$$

$$B = \frac{\alpha}{\tau_{LD}} \left(\frac{d}{d\omega} \ln r(\omega) \right). \tag{6}$$

After substituting Eq. (1) into Eq. (6) , the expression of B is then written as

$$B = \frac{\alpha}{\tau_{LD}} \left(\frac{d}{d\omega} \ln r_3(\omega) \right). \tag{7}$$

In Eq. (5) and Eq. (7), $\tau_{LD} = 2n_{g1}L_1/c$ is the roundtrip time in the solitary diode. The term A can be physically interpreted as the ratio between the external cavity optical length and the solitary diode optical length, which describes a linewidth reduction resulting solely from the extension of the cavity length. As described above, $\phi_{eff}(\omega)$ contains the effect of propagation in the waveguides to and from the MRRs. It also contains (via a maximum of $\frac{d}{d\omega}\varphi_{eff}(\omega)$ at the peak of the filter resonance) the cavity length enhancement resulting from multiple roundtrip passes through the MRRs. The term B describes an additional linewidth reduction that occurs only at the rising edge of the Vernier filter's reflection peak, where $\frac{d}{d\omega} \ln r(\omega)$ is positive.

The problem with the Schawlow-Townes expression in Eq. (3) is that it is based on the standard mean-field approach, which treats any lumped mirror loss as uniformly distributed along the cavity. However, such treatment is only valid for diode lasers that have symmetric and relatively high reflectivities ($r_1 \approx r_2 \approx 1$) such that the diode internal intensity is approximately uniform (spatially homogeneous). It should be noted that only with such uniform intensity, the carrier density is uniform as well, which is required to justify a uniform gain-index coupling in the form of the simple space-independent α-factor in Eq. (3). Hybrid lasers, specifically, do not generally fulfill these assumptions because the chip-to-chip coupling efficiency, β, might be rather low (at the 10% level without adiabatic tapering [20]), because the circuit reflectivity might be low and because the back facet reflectivity might also be very low, for instance, for the purpose of extracting more usable output power [24]. In these situations, the reflectivities of the equivalent solitary FP laser can become highly asymmetric, and the α-factor may strongly vary throughout the amplifier, which can increase the laser linewidth to beyond what is predicted in Eq. (2).

The limitations of the mean-field approximation had been realized by several independent researchers [25–27]. Specifically, lumping strongly asymmetric and low facet reflectivities in the Schawlow-Townes expression in Eq. (3) underestimates the coupling of amplified spontaneous emission into the main laser modebecause low facet reflectivities result in a large single pass gain. To take these effects into account to some extent, it was suggested [25–27] to modify Eq. (2) with another multiplicative factor, F_R, called spontaneous emission enhancement factor, given by

$$F_R = \left[\frac{(r_1 + r_2)(1 - r_1 r_2)}{2 r_1 r_2 \ln(r_1 r_2)} \right]^2, \tag{8}$$

where in the case of an external cavity hybrid laser r_2 is substituted by $r(\omega)$ (modified mean-field model).

However, even though modifying Eq. (2) with F_R takes into account additional noise by locally less depleted gain, this still does not address the associated index-effect that would lead to an increased α-factor. What is required to quantify this effect, for the first time in hybrid lasers, is to conduct detailed calculations which also include the spatially varying index effect in the laser linewidth.

Optics EXPRESS

4. Spatially resolved modeling of a hybrid laser

4.1. Implementation of the transmission line model

In order to conduct a more detailed and accurate linewidth analysis, which includes the spatial variations of the gain and index, we have chosen to apply an advanced transmission line model (TLM) for the gain section. Summarized, the implementation of the TLM [16,17] is a time-domain model that iterates optical fields travelling back and forth along the semiconductor amplifier to generate optical waveforms at the facets. Both the time and space coordinates are taken as discrete variables. Figure 2 shows the structure of the implemented TLM. The active gain section is divided into multiple short longitudinal TLM sections, each of which is short enough to be treated as homogeneous. For an efficient implementation, the TLM sections were chosen to have a length that is equal to the distance the light propagates within a model time step, $\Delta z = c\Delta t/n_{g1}$. For each section there is a so-called *scattering node* that represents, e.g., the electric field, carrier density, gain, loss and noise being present at that local section. Within each section, uncorrelated spontaneous emission noise is added as Langevin noise sources [7] for both forward and backward fields. The spectral shape of the spontaneous emission is determined by the gain spectrum, and the power spectral density is proportional to the local carrier density. The passive external resonator section is modeled in the frequency domain based on the scattering-matrix method [28] which makes use of well-known analytical solutions of the involved basic optical components, such as straight waveguide sections, Y-junctions, microring resonators [29–31]. A Fourier transform is performed in order to switch between the time-domain calculation and frequency-domain calculation. The configuration parameters for numerical modeling are given in Table 1. The laser parameters introduced into the TLM are summarized in Table 2 (diode parameters) and Table 3 (feedback parameters). The reason for our particular choice of parameters is that it enables a comparison of the numerically calculated linewidth with previously measured, experimental values as obtained with an according hybrid laser [32]. The first part of parameters is taken from the geometric and feedback waveguide parameters of that experimental setup. The remaining parameters are typical (standard) values for InP semiconductor amplifiers, which is why they are implemented also in the library of the used, commercially available TLM code [15].

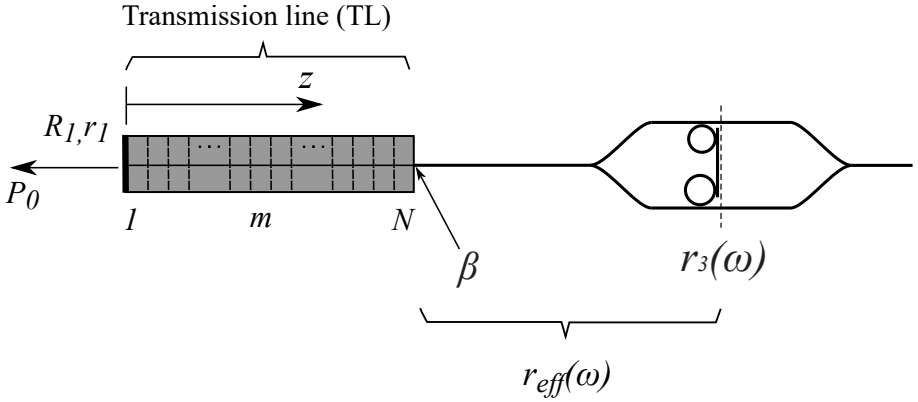

Fig. 2. Schematic representation of the transmission line model (TLM) for the hybrid laser. In the TLM applied here, the semiconductor gain medium is divided in sections. The passive external resonator section is modeled in the frequency domain based on the scattering-matrix method. $r_{eff}(\omega)$ is complex-valued and frequency dependent to include all frequency dependencies and phase shifts.

The goal is to model the propagation and amplification of waves at frequencies of hundreds of THz, however, this would require numerically unfeasible sampling rates of about a petahertz if

Optics EXPRESS

trying to resolve each optical cycle to full detail. To avoid this problem, we follow an alternative solution where the waves are modeled as a carrier wave (with a fixed, known frequency) multiplied with a somewhat slower varying envelope. This approximation is justified because the laser gain bandwidth is only a small fraction, about 5%, of the laser center frequency. In all of our modeling the center frequency was set to f_0 = 193.1 THz, which is equivalent to an output wavelength around 1550 nm. Each calculation run includes a large number of iterations, called scattering steps, taking place depending on the sample rate and the time window settings. Multiple runs can be carried out subsequently, each one taking as the initial values the last results of the former run. For the continuous-wave, steady-state laser modeled here, results from initial runs containing laser startup and transients can be discarded, and results from remaining runs, after the laser reaches steady-state, can be used for averaging of the frequency noise spectra.

In order to illustrate what feedback ($r_{eff}(\omega)$) we use in the numerical model, we plot in Fig. 3(a) the magnitude of r_{eff}, $r(\omega) = |r_{eff}|$, as obtained with the parameters in Table 3 for three different values of β ($\beta = 0.1, 0.5$ and 1). In Fig. 3(b) we plot the values for A, B and F, assuming a typical value for the linewidth enhancement factor, $\alpha = 3$. As the laser will operate at a frequency around the Vernier peak frequency (f_0), the horizontal axis is normalized to show the light frequency as a detuning with respect to f_0. It can be seen in Fig. 3(a) that the MRRs generate a spectral feedback maximum at zero detuning, where the height of the maximum decreases in proportion with β. The linewidth reduction terms A and B, which are associated with a spectrally varying phase ($\phi_{eff}(\omega)$) and amplitude ($r(\omega)$) of the feedback, and the resulting total linewidth reduction, F, are plotted in Fig. 3(b). It can be seen in Fig. 3(b) that the MRRs' spectrally filtered feedback causes a) a linewidth reduction brought by an enhanced cavity length due to multiple roundtrips (see peak of A at zero detuning); b) a linewidth reduction in the lower-frequency wing of the filter resonance (see asymmetric peak in B).

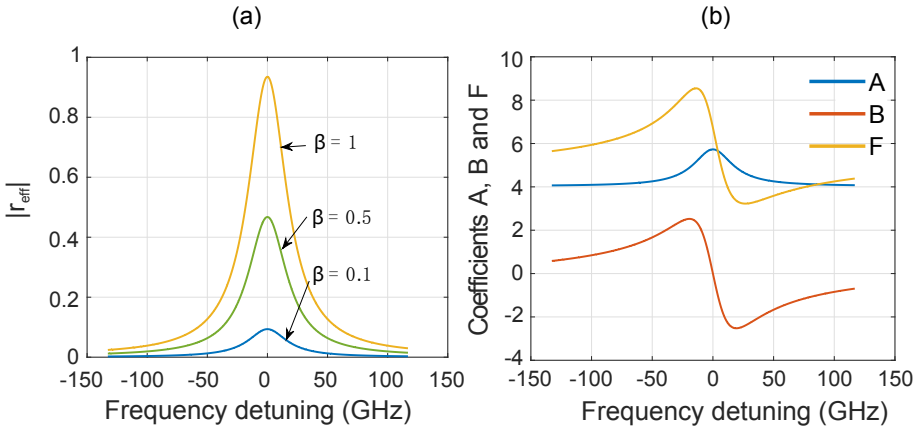

Fig. 3. (a) Calculated amplitude reflectivity as a function of frequency detuning (with respect to the Vernier peak frequency) for three different values of the chip-to-chip coupling efficiency, β; (b) Calculated coefficients A, B and linewidth reduction factor F as a function of frequency detuning. The values of A, B, and F are independent of the chip-to-chip coupling efficiencies.

In the following sections, we present typical results obtained from the numerical transmission line model and compare them with what is predicted by the modified mean-field model as given by Eqs. (2)-(8). In brief, we show that the two models agree well with each other, however, that the mean-field model underestimates the linewidth for the case of weak coupling between the two chips.

Optics EXPRESS

4.2. Output power and laser emission frequency

With the TL model, the output power (P_0) from the diode back facet and laser emission frequency (Δf, relative to f_0) was calculated for a range of coupling coefficients, from β = 0.1 to 1.0 in steps of 0.1, and for various different drive currents (I) up to 100 mA. Examples of typical results are presented in Fig. 4 (P *vs* I) and in Fig. 5 (Δf *vs* I), for three different coupling efficiencies, β = 1, 0.7, 0.3. It can be seen in Fig. 4 that the output power follows an approximately linear growth with the current interrupted by discontinuous hops, and that the overall power level drops as β decreases. Discontinuities are also seen in the output frequency (Fig. 5) and these occur at the same current values as in Fig. 4. Variations of the output frequency of lasers as in Fig. 5 are actually well known. They represent so-called mode hopping of the laser frequency to that of a neighboring longitudinal mode of the overall hybrid laser cavity. The frequency change of such a hop is given by the free spectral range (longitudinal mode spacing) of the hybrid laser cavity which is here approximately 14 GHz.

It can also be seen in Fig. 5 that between mode hops the frequency increases linearly with the drive current (such as the output power in Fig. 4). This might be understood follows: at higher drive currents, higher output powers and photon densities are reached. This results in a lower differential gain parameter and thus a higher carrier density for balancing the same threshold gain. A higher carrier density results in a lower refractive index [33], which leads to an increased laser frequency.

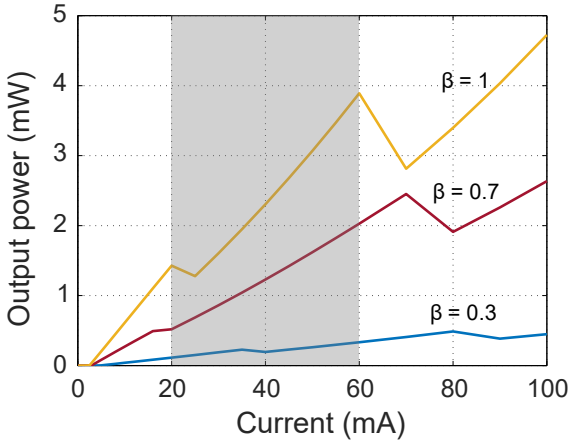

Fig. 4. Calculated output power *vs* drive current for three different values of the power coupling efficiency, β. The curves resemble the typical output power characteristic of diode lasers and the observed discontinuities are due to mode hopping. The values of the output power within the gray area (drive currents between 20 mA and 60 mA) were chosen for calculations of the linewidth (Fig. 7 and 8).

4.3. Frequency noise spectra and laser spectral linewidth

In order to calculate the laser spectral linewidth in a computationally feasible way, we calculate the power spectral density (PSD) of the frequency noise instead of directly resolving the full width at half maximum of the laser field power spectrum, because the latter requires kHz-level resolution and consequently a prohibitively long calculation time. The PSD is obtained via squaring the Fourier transform of the temporally varying (instantaneous) laser frequency. The fundamental (quantum) noise limited spectral linewidth can be retrieved from the limit value of the PSD as the noise frequency approaches zero, i.e., from the PSD in the flat, low-frequency part

Optics EXPRESS

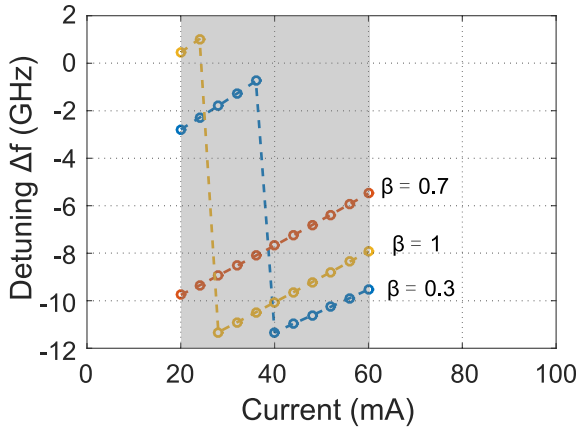

Fig. 5. Calculated laser frequency detuning Δf from the Vernier peak frequency (f_0) *vs* drive current for three different values of power coupling efficiency β. The frequency detuning and mode hops *vs* increasing drive currents are caused by index changes within the gain section.

of the noise spectrum [34]. Two examples of such frequency noise spectra are shown in Fig. 6, calculated for the same value of the chip-to-chip coupling ($\beta = 0.7$) but for two different drive currents (20 mA and 60 mA). In both spectra, two peaks can be seen. The first, shallower and broader peak corresponds to damped relaxation oscillations (between 2 and 3 GHz). The second, higher and narrower peak corresponds to beating between adjacent longitudinal modes (at about 14 GHz). It can be seen that the average PSD value at low frequencies (below 1 GHz) decreases from about $10.25 \times 10^3 Hz^2/Hz$ at 20 mA to about $2.36 \times 10^3 Hz^2/Hz$ at 60 mA, indicating (via multiplication by π [34]) a linewidth reduction from about 32.2 kHz to about 7.4 kHz.

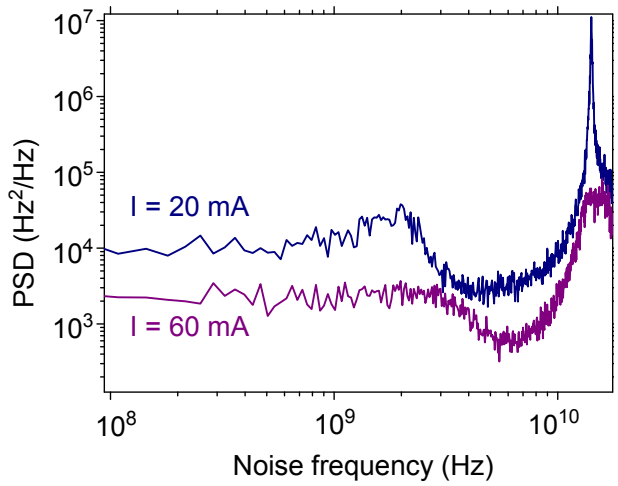

Fig. 6. Two examples of the calculated power spectral density (PSD) of frequency noise for power coupling efficiency $\beta = 0.7$ at 20 mA and 60 mA drive current. For each PSD curve, two spectral peaks can be seen, which correspond to relaxation oscillations (between 2 and 3 GHz) and beating between two adjacent longitudinal modes (at about 14 GHz) respectively. The laser spectral linewidth is retrieved via multiplying the mean values of the PSD at low frequencies by π, in this case obtaining about 32.2 kHz at 20 mA and 7.4 kHz at 60 mA.

Optics EXPRESS

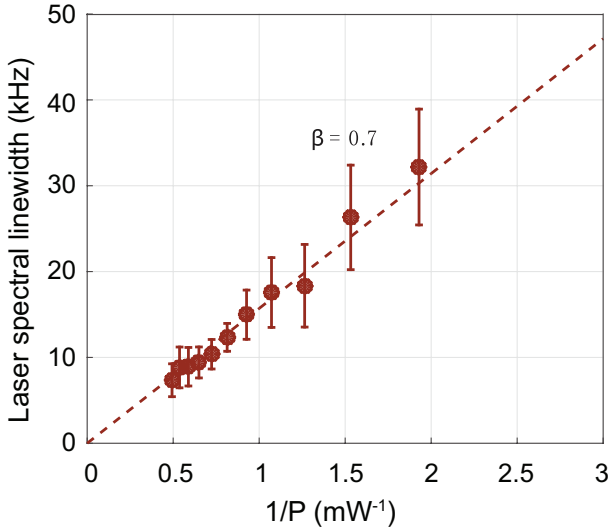

Fig. 7. Calculated laser spectral linewidth plotted *vs 1/P* for a chip-to-chip coupling efficiency $\beta = 0.7$, as an example. The symbols represent the values calculated with the transmission line model and the error bars represent the standard deviation of the PSD levels at low frequencies from the average PSD level in that range. The dashed line is a linear least mean square fit. The good agreement confirms the expected overall trend of linewidth narrowing with increasing output power. .

In order to conduct a first, qualitative comparison between the linewidth values from the transmission line model and the values obtained with the modified mean-field model, the linewidth for $\beta = 0.7$ is plotted as a function of the inverse output power, $1/P$, in Fig. 7. The motivation for plotting the linewidth *vs 1/P* is that Eq. (3) predicts a $1/P$ dependence. The symbols in Fig. 7 represent values calculated with the transmission line model and the error bars represent the standard deviation of the PSD at low frequencies from the average PSD in that range. The dashed line is a least mean square fit with a straight line as expected from Eq. (2). The numerical data clearly confirm the expected overall trend of linewidth narrowing with increasing output power, i.e., towards smaller values of $1/P$ on the horizontal axis. All other linewidth data calculated for other values of β (not shown here) displayed the same power dependence as long as no mode hop was present within the inspected range of power variation.

4.4. *Comparison between numerical results and analytical results*

To carry out a quantitative comparison between the numerically calculated linewidths and linewidths predicted by the mean-field theory, it is crucial to determine from the transmission line model an effective value of the linewidth enhancement factor, α, because, different from the analytical theory, such linewidth enhancement factor cannot be inserted a priori as parameter in the numerical model. Instead, the numerical model calculates explicitly the time dependent local carrier density, $N(z,t)$, from which it explicitly calculates the local refractive index, $n(z,t)$, and the according enhancement in laser frequency excursions. This means that, in the numerical model being much closer to a complete description, there is no generally valid α-factor. Instead the gain-index coupling is a local, space-dependent parameter of which some overall, effective (space averaged) α-factor may be derived that depends on the specific carrier and intensity distribution in the gain section. However, if the steady-state carrier density along the diode section is computed as a function of current at different values of β, this enables a calibration of the effective value of α comparable to the value of α-factor in the mean-field model, making use of

Optics EXPRESS

the fact that α is linearly proportional to the carrier density.

We have carried out the named calibration as follows: at first, an operation point is identified in terms of drive current that gives rise to steady-state operation and that satisfies the mean-field approximation. Here we chose $\beta = 1$ because then $r(\omega)$ is close to unity as well (see Fig. 3(a)), as is r_1 ($r_1 = 0.92$). As a result, the carrier density, N_0, shows a negligible spatial variation. Secondly, Eq. (2) is fitted to the linewidth obtained from the transmission line model, where α is the only fit parameter. For a drive current of 20 mA, this yields an α-value of 3.4, which we denote as α_0. In a third step, we obtain α-values for lower values of β via multiplying α_0 by N/N_0 where N is the spatially averaged carrier density, regardless of how strong the spatial variation is. As the last step, the theoretical linewidth value ($\Delta\nu$) obtained with Eqs. (2-8) is calculated, where the α-value from the previous step is inserted.

In Fig. 8, the ratio between the linewidth from the transmission line model and from the modified mean-field model, denoted as $\Delta\nu_{TL}/\Delta\nu$, is plotted as a function of $r(\omega)$ across the inspected range of β (0.1 to 1) and across the inspected range of drive currents (20 mA to 60 mA). It can be seen in Fig. 8 that at $r(\omega) \approx 1$ this ratio is approximately unity (at the calibration point as expected) but that it deviates increasingly from unity as the effective reflectivity decreases. The vertical spread of data points can be associated with uncertainties in linewidth retrieval from frequency noise spectra. Nevertheless, clearly an overall increasing trend of the ratio towards small values of $r(\omega)$ can be seen. For convenient practical use in predicting the influence of $r(\omega)$ on the laser linewidth also for other hybrid lasers, without the need to perform an extensive numerical modeling again, we have summarized the numerical data in a closed-form expression which we call a linewidth correction factor, F_c. The closed form is obtained by fitting a heuristic function with matching shape to the numerically calculated data in Fig. 8, under the assumption that Fc is equal to 1 when $r(\omega) \approx 1$ for physical correctness. The fitted function in the form of a simple exponential is given by

$$F_c = 0.94 + 1.06 \cdot \exp(-3.06 r(\omega)) \tag{9}$$

and may be used as an additional multiplicative factor in Eq. (2) to take non-unity effective reflectivity (e.g., induced by non-ideal coupling) into account to estimate the spectral linewidth of hybrid lasers.

5. Conclusion

Our theoretical modeling provides for the first time a comprehensive comparison between the existing, analytical linewidth theory (a modified-field model) and numerical calculations based on an advanced, spatially resolved transmission line model for hybrid diode lasers with frequency-selective feedback. It is found that with a weak optical coupling between the diode amplifier and the feedback (here a waveguide circuit on a chip), the modified mean-field model tends to underestimate the laser spectral linewidth. This underestimation becomes more apparent with decreasing coupling. We ascribe the discrepancy between the transmission line and mean-field model mainly to an inadequacy of the mean-field model in scaling the effect of a locally varying gain-index coupling into a single number for the α-linewidth enhancement factor.

While the direct implications of strong spatial gain variations may be well-included in the mean-field model via a spontaneous emission enhancement factor, this does not account for the associated variation in index. Our numerical modeling reveals that these index effects can be seen as an effective α-factor that increases the laser linewidth with decreasing feedback strength, and that the increase can be approximately accounted for with a heuristic linewidth correction factor, $F_c = 0.94 + 1.06\exp(-3.06 r(\omega))$, where $r(\omega)$ is the coefficient that describes the effective amplitude reflectivity of the feedback circuit.

Our findings have the following implications for predicting the spectral linewidth of hybrid lasers in order to find a proper design of the waveguide feedback circuit parameters before

Optics EXPRESS

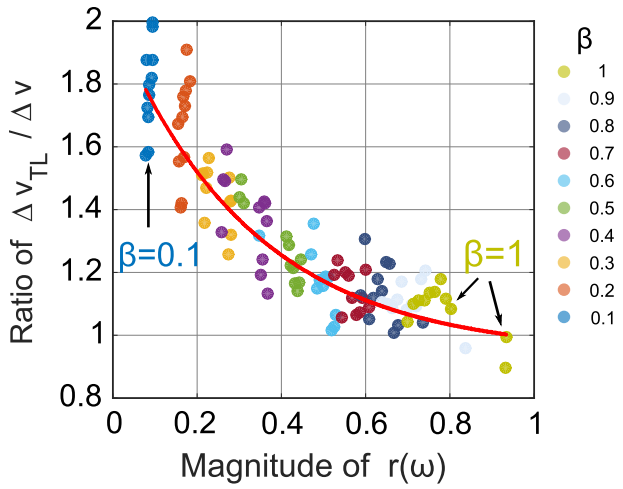

Fig. 8. Ratio between laser spectral linewidths obtained with the transmission line model and the modified mean-field model for the full range of power coupling efficiencies β (0.1 to 1) and drive currents (20 mA to 60 mA). Due to the different amount of laser frequency detuning caused by different drive currents, $|r(\omega)|$ varies with drive current for each value of β. A systematic decrease of $|r(\omega)|$ can be seen as β decreases from unity (1) to a low value of 0.1, which can be understood by Eq. (1) where β enters $|r(\omega)|$ as a multiplicative factor. The red solid curve is a simple exponential fitting curve. A clear trend of increasing error in the mean-field model is seen when β approaches smaller values.

fabrication and hybrid integration:

1. For a proper prediction of the laser linewidth in the case of strong feedback (β close to unity), it is fully sufficient to use the current, modified mean-field theory as guidance. The laser linewidth will decrease as expected with increasing output power, with increasing mode coupling efficiency, and by implementing feedback circuits with low loss and a large linewidth reduction term (F^2 in Eq. (4));

2. For hybrid lasers with weak coupling ($\beta \leq 0.1$) where a strong spatial variation in the carrier density is present, the analytical theory should be applied with more caution although the laser linewidth still decreases with increasing output power. Namely one should be aware that the presence of a strong spatial variation in carrier density will broaden the linewidth due to an additional index related effect. For instance, at a weak coupling of $\beta = 0.1$ (which is still fully sufficient for laser operation due to the huge gain provided by diode amplifiers) the linewidth will be larger by a factor of about 2.

Examples of the second situation are hybrid lasers where the feedback mode is not well matched to the diode waveguide mode, or when the feedback waveguide circuit itself is providing high losses, such as would typically occur with feedback from waveguide circuits fabricated from Si. Also other types of diode lasers show a strong variation of the carrier density and should thus exhibit linewidths larger than expected. These are diode lasers that are deliberately equipped with a low reflectivity of the back facet (at the few percent level or below) [24] as is often chosen to increase the usable output power, or heterogeneous integrated hybrid DFB lasers [35] that might show strong spatial carrier density variations such as through spatial hole burning [12].

Optics EXPRESS

6. Appendix

6.1. Model descriptions

In this section we briefly recall [7, 36–40] the basic equations for the TLM model that is used in the diode gain chip. The electric field inside each TLM section, $E(z,t)$, can be represented as

$$E(z,t) = f(z,t) + b(z,t), \tag{10}$$

$$f(z,t) = F(z,t)e^{-qz-i\omega_0 t}, \tag{11}$$

$$b(z,t) = B(z,t)e^{+qz-i\omega_0 t}, \tag{12}$$

where $F(z,t)$ and $B(z,t)$ are the complex envelopes for the forward and backward propagating field respectively [36], q is the propagation constant, and ω_0 is the operating center angular frequency. The field propagation is described by the following two coupled equations [37]:

$$\left(\frac{1}{v_g} + \frac{\partial}{\partial z}\right) f(z,t) = \left(\frac{1}{2}g - \frac{1}{2}\alpha_i\right) f(z,t) + Q_{spf}, \tag{13}$$

$$\left(\frac{1}{v_g} + \frac{\partial}{\partial z}\right) b(z,t) = \left(\frac{1}{2}g - \frac{1}{2}\alpha_i\right) b(z,t) + Q_{spb}, \tag{14}$$

where v_g is the group velocity; α_i is the internal loss; Q_{spf} and Q_{spb} are stochastic Langevin noise terms [7] caused by spontaneous emission that is coupled into the propagation fields; g is the modal gain and its dependency on carrier density and photon density (S) can be found in [38], and is given by

$$g = \frac{\Gamma g_0 \ln(N_{MQW}/N_{tr})}{1+\epsilon S}. \tag{15}$$

where Γ is the modal confinement factor; g_0 is the gain coefficient; N_{tr} is the transparency carrier density; and ϵ is the gain compression factor. The carrier dynamics is governed by the following two coupled rate equations:

$$\frac{dN_{SCH}}{dt} = \eta_i \frac{I}{ewL_1 d_{SCH}} - \frac{N_{SCH}}{\tau_{cap}} + \frac{N_{MQW}}{\tau_{em}} \cdot \frac{d_{MQW}}{d_{SCH}}, \tag{16}$$

$$\frac{dN_{MQW}}{dt} = \frac{N_{SCH}}{\tau_{cap}} \cdot \frac{d_{SCH}}{d_{MQW}} - \frac{N_{MQW}}{\tau_{em}} - v_g g S - R(N_{MQW}). \tag{17}$$

$$R(N_{MQW}) = A_d N_{MQW} + B_d N_{MQW}^2 + C_d N_{MQW}^3. \tag{18}$$

which involves two carrier densities, i.e., one in the separate-confinement heterojunction (SCH) layer, N_{SCH}, and the other in the multiple quantum wells, N_{MQW}. The coefficients A_d, B_d, and C_d describe the single-electron recombination, bimolecular and Auger recombination, respectively [37]. The two cross sectional areas exchange carriers with each other at time scales that are determined by two time constants (capture time τ_{cap} and thermionic emission time τ_{em}) [39, 40].

6.2. Numerical parameters

Optics EXPRESS

Table 1. Configuration parameters used for numerical modeling

Symbol	Value	Description
BW	10.24 THz	Sampling rate
T	25.6 ns	Time window for each calculation
Ave	10	Number of averages for each PSD spectrum

Table 2. Semiconductor chip parameters

Symbol	Value	Description
e	$1.6 \cdot 10^{-16}$ J	Elementary charge
λ	1552.6 nm	Operating wavelength
g_0	1800 cm^{-1}	Gain coefficient
N_{tr}	$1.5 \cdot 10^{18}$ cm^{-3}	Transparency carrier density
ϵ	$1 \cdot 10^{-17}$ cm^3	Gain compression factor
η_i	1	Internal efficiency
A_d	0	Linear recombination coefficient
B_d	$1.0 \cdot 10^{-10}$ cm^3/s	Bimolecular recombination coefficient
C_d	$1.3 \cdot 10^{-29}$ cm^6/s	Auger recombination coefficient
n_{g1}	3.6	Group index of laser diode material
L_1	400 μm	Length of active layer
d_{MQW}	40 nm	Total thickness of the multiple quantum wells
d_{SCH}	200 nm	Total thickness of the SCH layers
τ_{cap}	70 ps	SCH capture time
τ_{em}	140 ps	MQW thermionic emission time
w	2.5 μm	Width of active layer
R_1	0.85	Left facet power reflection
R_2	0	Right facet power reflection
α_i	1607 m^{-1}	Internal loss coefficient of the laser diode
n_{sp}	2.0	Spontaneous emission coefficient at threshold
Γ	0.07	Optical confinement factor of the MQW area

Table 3. Feedback waveguide chip parameters

Symbol	Value	Description
S_1	49.5 μm	Radius of the first microring resonator
S_2	54.0 μm	Radius of the second microring resonator
α_2	60 dB/m	Waveguide attenuation
κ^2	0.2	Power coupling coefficient for both MRRs
L_2	3500 μm	Bus waveguide length
n_{eff2}	1.54	Effective index
n_{g2}	1.7147	Group index

Funding

Rijksdienst voor Ondernemend Nederland (RVO) (IPD12009); Dutch Technology Foundation STW (10442).

Optics EXPRESS

Acknowledgment

This work is supported by funding within the framework of the Promis2Day project, for which the authors gratefully acknowledge the support of the IOP Photonic Devices program of Rijksdienst voor Ondernemend Nederland (RVO), part of the Netherlands Ministry of Economic Affairs and the Netherlands Ministry of Education, Culture and Science. This work is also partly supported by the Dutch Technology Foundation STW, which is part of the Netherlands Organization for Scientific Research (NWO). We thank Julien Javaloyes (Universitat de les Illes Balears, Spain) for fruitful discussions.